CrystEngComm

Cu2O nanoparticle catalyzed synthesis of diaryl tetrazolones and investigation of their solid-state properties

Journal:	*CrystEngComm*
Manuscript ID	CE-ART-01-2021-000119.R1
Article Type:	Paper
Date Submitted by the Author:	07-Mar-2021

Complete List of Authors:	Reason, Thomas; Ball State University, Chemistry Goka, Benjamin ; Ball State University College of Sciences and Humanities Krause, Jeanette; University of Cincinnati, Chemistry Fionah, Abelline; Ball State University, Chemistry Zahran, Elsayed; Ball State University, Department of Chemistry; National Research Centre , Rayat, Sundeep; Ball State University, Chemistry

Cu_2O nanoparticle catalyzed synthesis of diaryl tetrazolones and investigation of their solid-state properties.

Thomas E. Reason,[†] Benjamin Goka,[†] Jeanette A. Krause[‡], Abelline Fionah,[†] Elsayed M. Zahran[†], and Sundeep Rayat[†]*

[†]*Department of Chemistry, Ball State University, Cooper Physical Science Building, Muncie, IN 47304 - 0445, USA.*

[‡]*Department of Chemistry, University of Cincinnati, Cincinnati, Ohio 45221-0172, United States*

Abstract

An efficient and versatile method for the synthesis of 1,4-diaryl tetrazolones **1** is reported which involves C-N coupling of aryl tetrazolones **2** with aryl boronic acids **3** in the presence of Cu_2O nanoparticles under an oxygen atmosphere and DMSO as solvent. The reaction tolerates a variety of electron donating and electron withdrawing substituents on both substrates and produces the desired 1,4-diaryl tetrazolones **1** in moderate to good yields. In the crystal lattice, the molecules exhibit π..π stacking interactions between the adjacent layers as well as weak through-space electrostatic C-H…O interactions involving the pendant rings and tetrazolone carbonyl. 1-(4-Methoxyphenyl)-4-(3-tolyl)-1,4-dihydro-5*H*-tetrazol-5-one **1bk** and 1-(3-fluorophenyl)-4-(4-methoxyphenyl)-1,4-dihydro-5*H*-tetrazol-5-one **1be**, differing only in the presence of one group (methyl or fluoro), exhibited an identical pattern of noncovalent interactions in the solid-state. Hirshfeld surface analyses has also been performed to visualize intermolecular interactions.

Introduction

Tetrazolone is an important structural motif with broad significance in medicine, agriculture, and material science. In medicine, tetrazolone derivatives are found to be rho-kinase inhibitors,[1] monoacylglycerol acyltransferase type 2 inhibitors,[2] fatty acid synthase inhibitors,[3] cannabinoid receptor 2 agonists,[4] α2C-adrenoreceptor antagonists,[5] β3 adrenergic receptor agonists.[6] As a result, many tetazolone based drugs have been patented for cardiovascular, smooth muscle, neuropathological, autoimmune, fibrotic, and inflammatory diseases as well as for treatment of cancer, obesity, diabetes and sexual dysfunction.[1-6] Recently, the tetrazolone scaffold has been recognized as a carboxylic acid bioisostere[7] as the substitution of a -COOH group in a marketed anti-hypertensive drug, with a tetrazolone ring, produced a more potent analog. In agriculture, tetrazolone is one of the key motifs used for the design of effective fungicides[8], herbicides[9, 10] and insecticides.[11, 12] In materials chemistry, the parent tetrazole ring has been widely utilized in the design of coordination compounds and metal organic frameworks (MOFs).[13-15] However, tetrazolones have not received much attention in this area. For example, eight complexes of unsubstituted tetrazolone with alkali and alkaline earth metals have been recently reported as high energy materials.[16, 17] Two complexes of 1-methyl-5-tetrazolone with silver and palladium are known,[18] where the ligand binds to the metal ion at N4.

Most of the aforementioned work has focused on *N*-aryl,[7] *N,N*-dialkyl,[19, 20] *N*-aryl-*N*-alkyl,[6, 8, 9, 21] and *N*-aryl-*N*-triazole[11] derivatives of tetrazolones. On the other hand, reports on *N,N*-diarylated tetrazolones (or 1,4-diaryl tetrazolones) are limited. For instance, our group reported antiproliferative activity of 1,4-diaryl tetrazolones against L1210 leukemia and SK-BR-3 breast cancer cell lines *in-vitro*.[22] Recently, a few *N,N*-diarylated tetrazolones have been patented for

pesticidal use.[23] Quast and coworkers investigated the photodecomposition of 1,4-diaryl tetrazolones which results in the loss of dinitrogen and leads to the formation of benzimidazoles.[24, 25]

The dearth of investigations on *N,N*-diarylated tetrazolones may be attributed to the lack of robust and versatile synthetic techniques to obtain these target compounds. Previously, we have reported the synthesis of these compounds through a $Cu(OAc)_2$ mediated coupling of aryl tetrazolones with aryl boronic acids in the presence of pyridine and ambient air.[22] However, the reaction required a stoichiometric amount of the Cu catalyst and suffered from long reaction times and poor yields. Improved synthetic methods to obtain 1,4-diaryl tetrazolones are desirable to explore the applications of these structures in various fields.

Reports on the crystal structure of tetrazolones are also limited.[11, 26-32] Yet, knowledge of the solid-state packing of these compounds is critical due to their significance (a) in medicinal chemistry where the physical and chemical properties of an active pharmaceutical ingredient are dependent on its crystalline form,[33, 34] as well as (2) in materials chemistry where the noncovalent interactions between the neighboring molecules are the driving force in the assembly of unorganized molecules in solution into organized supramolecular architectures in the solid state.[15] Thus, understanding the crystalline structure of *N,N*-diarylated tetrazolones would be valuable in designing pharmaceuticals with better efficacy and functional materials with predictable topologies.

In this article, we report an improved method to synthesize 1,4-diarylated tetrazolones which involves Cu_2O nanoparticle-catalyzed aerobic oxidation of aryl tetrazolones and aryl boronic acids. We also report X-ray crystallographic analyses on select compounds in order to

provide insight into the nature of the intermolecular interactions responsible for the extended packing observed in the solid-state.

Results and Discussion

Han and coworkers have reported that Cu_2O catalyzed aerobic oxidation of the aryl tetrazoles with a variety of hetero(aryl) boronates in DMSO and in the absence of a base leads to the production of 2,5-diaryl tetrazoles.[35] We evaluated this procedure to synthesize 1,4-diphenyl-1,4-dihydro-5*H*-tetrazol-5-one **1aa** *via* the coupling of phenyl tetrazolone **2a**[36] with phenyl boronic acid **3a** (Table 1). To our delight, **1aa** was formed in 3.5 hours and in 80% yield (entry 2), a significant improvement over the previous method[22] which utilized a stoichiometric amount of $Cu(OAc)_2$ and required 44 hours of reaction time to produce **1aa** in 62% (entry 1). Solvent effects on this reaction were also investigated. Previous reports on the Cu-catalyzed cross coupling of tetrazoles with boronic acids have shown that DMSO is critical for success of the reaction. It is believed that the catalytic cycle involves coordination of copper to DMSO.[37] The coordination of DMSO to copper moieties to enhance catalytic potential has been documented for other reactions.[38, 39] It is reasonable to hypothesize that a similar catalytic cycle is involved in the *N*-arylation of phenyl tetrazolone **2a** with phenyl boronic acid **3a**. Replacement of DMSO with sulfolane, a structurally similar and a greener alternative, formed **1aa** in modest yield after 48 hours (entry 3). Increased reaction time and decreased the yield of **1aa** in this case may be attributed to the steric bulk of the sulfolane which could hinder its coordination to the copper. Substituting DMSO with ethanol, a polar protic solvent, produced only a trace amount of product after 48 hours as determined by TLC (entry 4), further emphasizing the coordination effect of the DMSO.

Nanoparticle catalysts show significantly enhanced reactivity and selectivity compared to their bulk form due to large surface area to volume ratio,[40-42] thus prompting us to investigate the effect of the size of Cu_2O nanocubes on the catalytic activity and reaction yields. Controlled low temperature hydrothermal approaches were used to prepare three different sizes of Cu_2O nanostructures: 100, 300 and 800 nm.[43, 44] Electron microscopy images were obtained to characterize the size and morphology of the Cu_2O cubes prepared by the various procedures (See Figure S1).

Table 1. Optimization of reaction conditions[a]

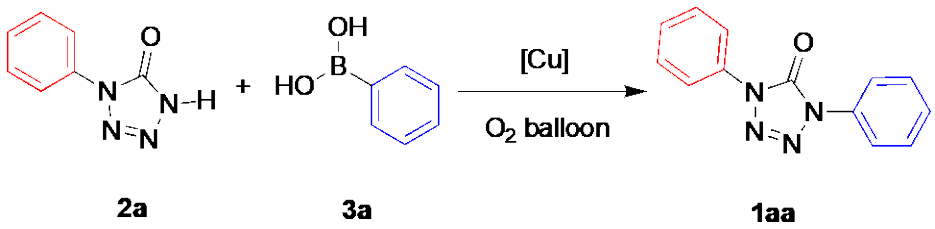

2a **3a** **1aa**

Entry	[Cu]	Size	mol%	Solvent	Time (h)	Yield (%)
1	$Cu(OAc)_2$[b]	amorphous	150%	CH_2Cl_2	44	62
2	Cu_2O	amorphous	5%	DMSO	3.5	80
3	Cu_2O	amorphous	5%	Sulfolane	48	45
4	Cu_2O[c]	amorphous	5%	EtOH	48	trace[e]
5	Cu_2O	100 nm	5%	DMSO	1	53
6	Cu_2O	300 nm	5%	DMSO	2	83
7	Cu_2O	800 nm	5%	DMSO	2	62
8	Cu_2O	300 nm	2.5%	DMSO	1.5	46
9	Cu_2O[d]	300 nm	5%	DMSO	24	trace[e]

[a]Reaction conditions unless otherwise indicated: **2** (1.0 mmol), **3** (2.0 mmol), and Cu_2O in DMSO (8 mL) at 100 °C; [b]Reaction conditions: **2** (1.5 mmol), **3** (3.0 mmol), pyridine (3.0 mmol, 2 equiv), $Cu(OAc)_2$ (2.3 mmol), molecular sieves (3Å, 0.8 g) in DCM (30 mL) stirred at room temperature in air; [c]Reaction carried out at 60 ºC and at [d]room temperature; [e]from TLC.

The different sizes of nanoparticles studied (entries 5 – 7) showed a decrease in overall reaction time (≤2 h) compared to the amorphous Cu_2O (entry 2). However, only the 300 nm Cu_2O nanocubes produced yields commensurate with the amorphous catalyst (entries 2 & 6), while the 100 and 800 nm nanoparticles (entries 5 & 7) resulted in decreased product yields. The reason for the limited activity of the 100 nm nanoparticles is not understood at this time. It may be due to the different oxidation state of the copper on the surface of the catalyst, however, further investigations are needed to verify this hypothesis. From these results, it was determined that 300 nm Cu_2O nanoparticles would be best to use for the formation of 1,4-diaryl tetrazolones. Using the 300 nm Cu_2O nanocubes, we also examined a lower catalyst loading (2.5 mol%) for coupling of **2a** and **3a**, but the yield suffered greatly compared to the meager half an hour reduction in the reaction time (entry 8). The reaction at room temperature produced only trace amounts of **1aa** after 24h (entry 9), as indicated by the TLC, which suggested that temperature plays an important role in the efficiency of this reaction. Note that Han et al. have shown that reaction of 5-phenyltetrazole with boronic acid in the absence of Cu_2O catalyst did not produce any product.[35] We expected a similar outcome for the reaction of **2a** with **3a**.

After the optimized conditions were determined, we set out to examine the scope of aryl tetrazolones **2** and a variety of boronic acids **3** (Table 2). Phenyl tetrazolone **2a** reacted with aryl boronic acids substituted with an electron-donating ethoxy group at the *para* and *meta* positions to give **1ab** and **1ac** in 60% and 87% yield, respectively (entries 2 and 3). The coupling reaction

also tolerated the presence of a weakly-deactivating fluoro group at the *para* and *meta* positions of the phenylboronic acid and produced **1ad** and **1ae** in excellent yields (entries 3 and 4). Note that these compounds were prepared in 60% and 21% yields, respectively, after many hours using the $Cu(OAc)_2$ method.[22] In comparison, the *ortho* substitution of the weakly-deactivating fluoro and bromo groups produced only trace amounts of tetrazolones **1af** and **1ag** after several hours, which may be attributed to steric hindrance encountered during coordination to copper in the catalytic cycle (entries 6 and 7). It is worth noting that **1ag** can be produced in 54% yield after 60h using the $Cu(OAc)_2$ method.[22] The presence of moderately and weakly electron-withdrawing carboxylic acid and nitro groups required prolonged reaction times and a messy extraction that led to loss of the product and thus, reduced yields of **1ah** and **1ai** (46 – 48%, entries 8 and 9). The versatility of this method was also examined for a heteroaryl boronic acid, specifically the 3-pyridyl boronic acid which produced **1aj** in moderate yield (51%, entry 10) upon reaction with **2a** after 24 hrs.

Next, we examined the *N*-arylation of substituted phenyl tetrazolones with boronic acids. Our work revealed that **2b** substituted with an electron-donating *para* methoxy group underwent coupling with phenyl boronic acid substituted with weakly activating (-Me) and deactivating groups (*m*-F and *p*-F) to give the corresponding 1,4-diaryl tetrazolones **1bk**, **1bd** and **1be** in 80% yield (entries 11 – 13). Similarly, the reaction of phenyl tetrazolone **2c** decorated with an electron-withdrawing nitro group with 3,5-dimethoxyphenyl- and (4-(diphenylamino)phenyl) boronic acids **3l** and **3m** was also successful and afforded both **1cl** and **1cm** in 77% yield (entries 14 and 15).

Table 2. C-N coupling of aryl tetrazolones 2 with aryl boronic acids 3[a]

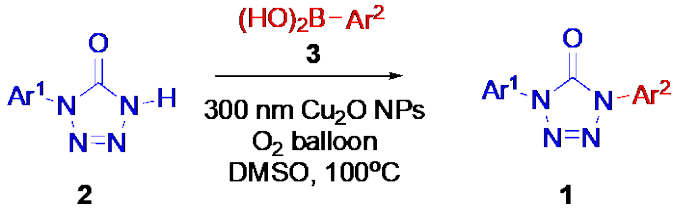

Entry	Compound	Structure	Time (h)	Yield (%)
1	**1aa**	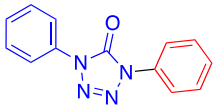	2(44[b])	83(62[b])
2	**1ab**	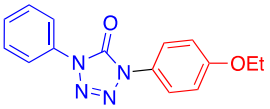	2	60
3	**1ac**	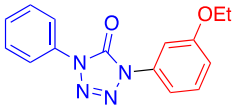	1.5	87
4	**1ad**	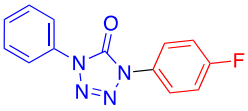	2(24[b])	81(60[b])
5	**1ae**	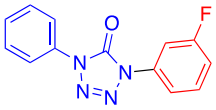	2(77[b])	76(21[b])
6	**1af**	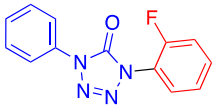	72	Trace [c]
7	**1ag**	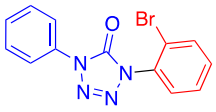	48 (60[22])	Trace[c] (54[22])
8	**1ah**	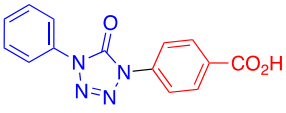	4 – 24[d]	48
9	**1ai**	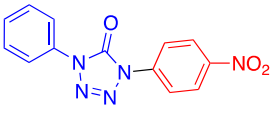	4 – 25[d]	46

10	**1aj**	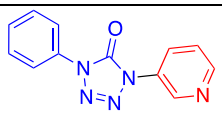	24	51
11	**1bk**	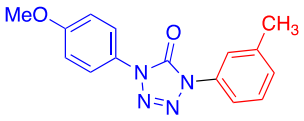	2(96[b])	80(16[b])
12	**1bd**	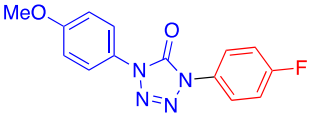	2	79
13	**1be**	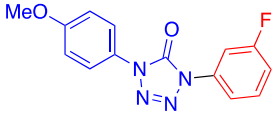	2(48[b])	80(23[b])
14	**1cl**	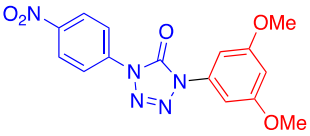	2.5	77
15	**1cm**	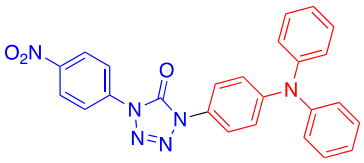	2.5	77

*[a]Reaction conditions unless otherwise indicated: **3** (1.0 mmol), **4** (2.0 mmol), and Cu_2O in DMSO (8 mL) at 100 °C. [b]Reaction conditions: **3** (1.5 mmol), **4** (3.0 mmol), pyridine (3.0 mmol, 2 equiv), $Cu(OAc)_2$ (2.3 mmol), molecular sieves (3Å, 0.8 g), in DCM (30 mL) stirred at room temperature in air; [c]from TLC; [d]Exact reaction time could not be determined due to limited access to the laboratory due to COVID-19 restrictions.*

Electrostatic Potential Calculations. We were successful in obtaining single crystals of six of the synthesized compounds which includes **1aa**, **1ac**, **1ad**, **1bk**, **1be and 1cl**. To understand the intermolecular interactions in the solid-state of these compounds, the structures were optimized at the M062X/6-311G* level of theory using Gaussian 09 package of programs.[45] The molecular

electrostatic potentials (MESP) plots and surface minima (Vs,min) were calculated and visualized using GaussView.[46] The MESP analysis shows that the greatest degree of negative charge (red region) is concentrated at the carbonyl oxygen and to a lesser extent near the N=N unit of the tetrazolone ring in these molecules, while positive charge (blue region) is concentrated at the centroid of the tetrazolone (Figure 1).

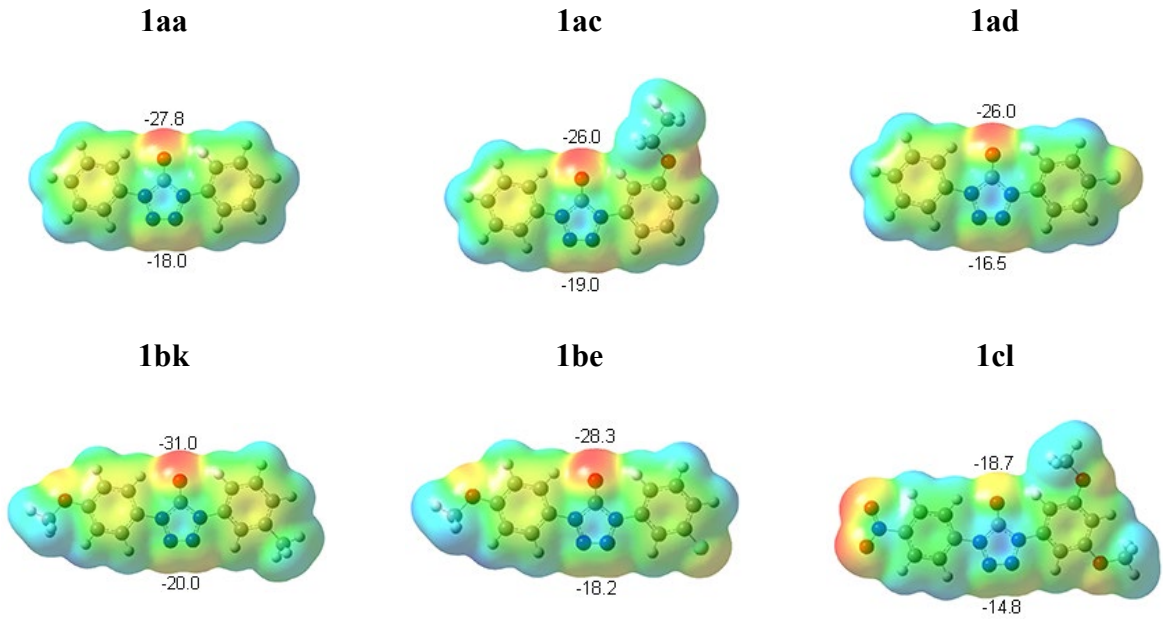

Figure 1. Molecular electrostatic potentials at 0.001 a.u. iso-surface of electron density for **1aa**, **1ac**, **1ad**, **1bk**, **1be** and **1cl**, calculated at M062X/6-311G*. The MESP values of the surface minima (Vs, min) at the selected points are in kcal/mol.

X-ray crystallography. The molecular structure diagrams and crystal data refinement details of **1aa**, **1ac**, **1ad**, **1bk**, **1be** and **1cl** are given in Figures S2-S8 and Tables S1-S7. **1aa** crystallized from dichloromethane in the tetragonal $P4_1$ space group as six independent molecules in the asymmetric unit. In contrast, **1ac**, **1ad**, **1bk**, **1be** and **1cl** crystallize as one independent molecule in the more common monoclinic or orthorhombic crystal systems. **1be** crystallized as either a

monoclinic C-centered polymorph from methanol (**1be$_{MeOH}$**) or a primitive monoclinic polymorph from acetonitrile (**1be$_{MeCN}$**). As expected, the individual rings in all the complexes are planar. The **1aa** pendant phenyl rings vary in dihedral angle relative to the central tetrazolone core (0.7(2)-19.7(2)°) with most molecules showing a slight twist in the position of the phenyl rings with respect to each other rather than a more planar or bowed molecular backbone (Figure S2). The molecular structure of **1ac** obtained in acetonitrile, shows small deviations from planarity, 2.43(8)° and 2.87(8)°, between the central ring and the substituents, giving the molecular backbone a planar geometry (Figure S3). **1ad** obtained from methanol crystallizes in the centrosymmetric space group Pnma with a slightly bowed arrangement between the central heterocycle and the pendant aryl rings (dihedral angle = 15.79(6)°) (Figure S4). A slight twisting adopted by the peripheral rings relative to each other is observed in **1bk** and both polymorphs of **1be** (Figures S5-S7) with dihedral angles clustered about 13 – 15° while **1cl** (Figure S8) shows more variation (8.9(1) and 17.1(1)°). All single crystal structures were overlayed that further show that the molecules exhibit different ring orientations associated with the pendant phenyl or substituted aryl moieties that can be described as twisting or bowing relative to the tetrazolone ring (Figure S5).

While the molecular structures of these complexes are rather straightforward, of interest are the extended stacking and intermolecular interactions. Examination of the extended packing structure of **1aa** revealed a layered stacking motif along the *c*-axis with varying tilt angles between the planes, however no identifiable structure-directing noncovalent interactions were observed. Inspection of the unit cell of **1ac**, revealed weak electrostatic C-H…O interactions involving an aromatic C-H of the 3-ethoxyphenyl moiety with the oxygen of a neighboring ethoxy group (2.52Å) as well as the C-H of the phenyl group with the oxygen of a neighboring tetrazolone ring (2.57Å). An overall slipped π-π interaction between adjacent layers is observed with a 3.33Å

distance between the stacked planes and a long distance (>4Å) between tetrazolone centroids (Figure 2).

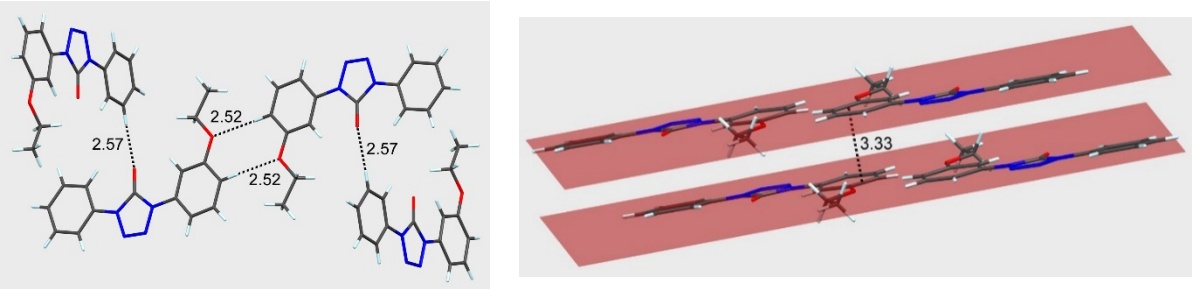

Figure 2. Left: C-H…O intermolecular interactions in the crystal lattice of **1ac**; right: interplanar stacking arrangement.

As deduced from the calculations, molecules **1ad**, **1bk** and **1be** pack by utilizing the electrostatic interaction between the positive and negative regions of the heterocycle. The negative potential encompassing the carbonyl oxygen of **1ad** is attracted to the positive potential at the center of the tetrazolone, a C=O…$N_4C_{centroid}$ interaction distance of 2.90Å is observed giving rise to a staircase motif in the solid state (Figure 3).

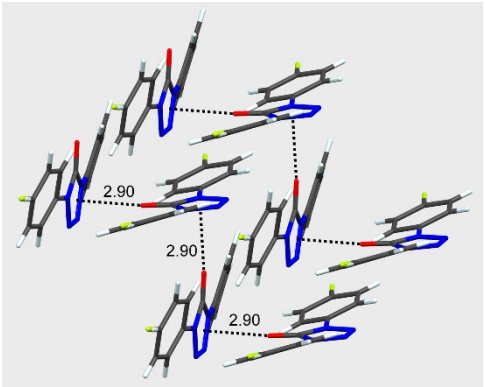

Figure 3. Intermolecular interactions in the crystal lattice of **1ad**.

1bk exhibits a π-π stacking motif with a least squares distance of 3.04Å, consistent with other complexes in this study (Figure 4). While the extended packing geometry may approximate a herringbone motif, the individual stacks support weak C-H…O interactions between neighboring methyl groups and either a methoxy or carbonyl oxygen atom ($C\text{-}H_{Me}..O_{OMe}$ = 2.70Å, $C\text{-}H_{OMe}…O{=}C$ = 2.53Å) rather than with the tetrazolone heterocyclic N_4C core.

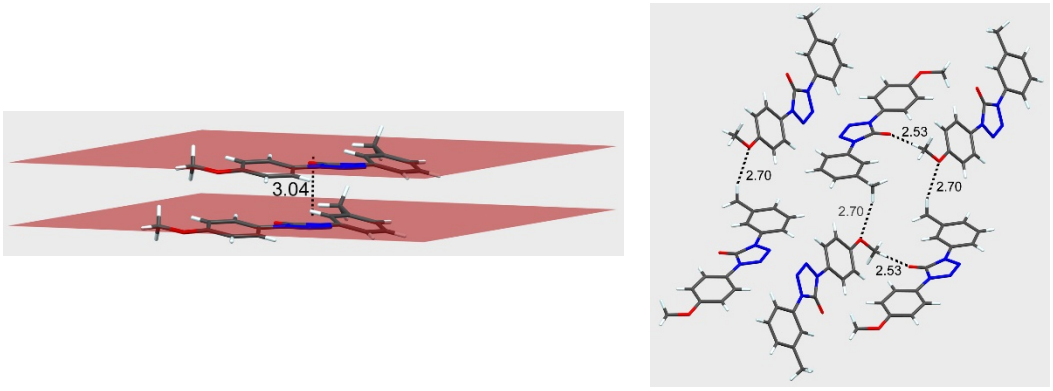

Figure 4. Interplanar (left) and intermolecular interactions (right) between molecules of **1bk** in the crystalline lattice.

Two polymorphs of **1be** result from methanol (**1be$_{MeOH}$**) or acetonitrile (**1be$_{MeCN}$**) crystallization (Figure 5). The noncovalent interactions observed for **1be$_{MeOH}$** approximate those of **1bk**, namely a π-π stacking of 3.02Å between the adjacent stacked planes and individual stacks held *via* C-H…F interactions involving the pendant aromatic rings. A somewhat longer, π-π stacking interaction, 3.12Å, is seen for **1be$_{MeCN}$** with a tetrazolone $N_4C_{centroid}…N_4C_{centroid}$ distance of 3.84Å indicative of a very weak, inefficient electrostatic attraction. One can conclude that the placement of the molecules is dictated by the C-H…O and C-H…F interactions rather than tetrazolone ring interactions for both crystals of **1be**.

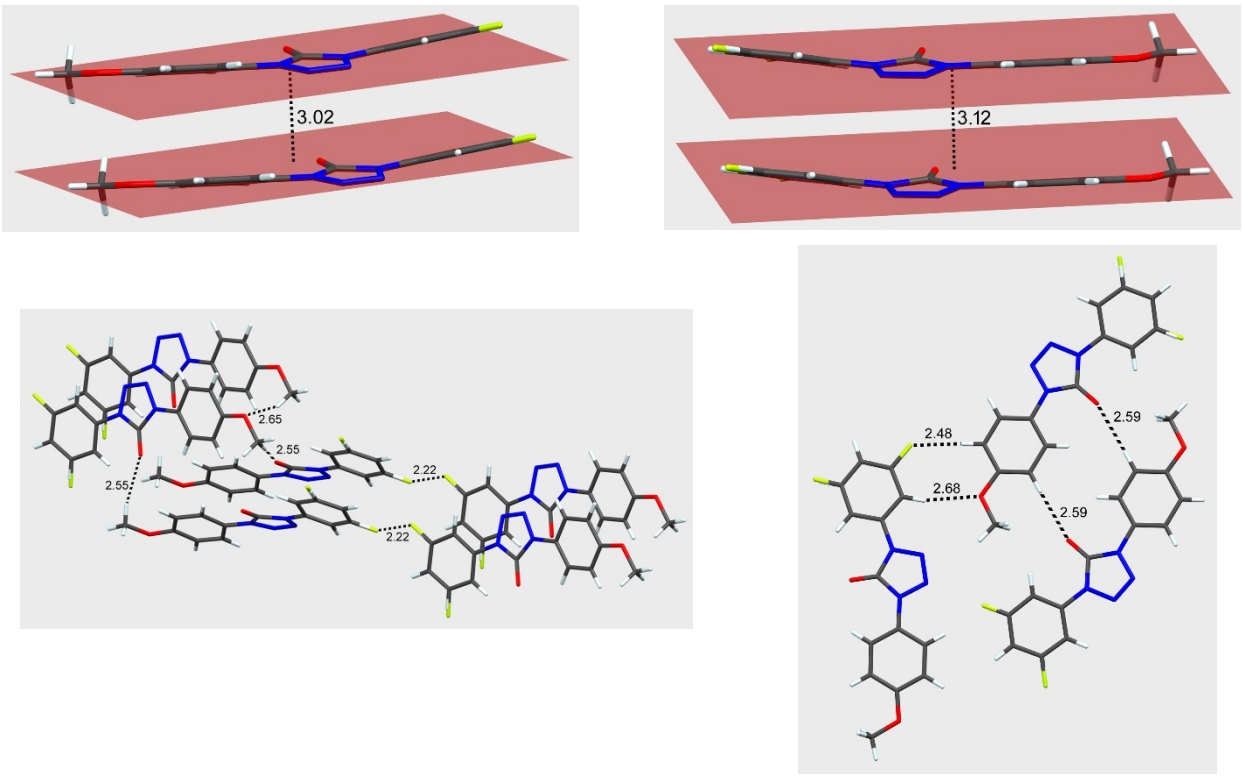

Figure 5. Comparison of the interplanar separations (top) and C-H…O intermolecular interactions (bottom) for the polymorphs **1be**$_{\mathbf{MeOH}}$ (left) and **1be**$_{\mathbf{MeCN}}$ (right).

1cl adopts a slipped pattern that has a large stacking distance and tetrazolone centroid-to-centroid ring separation (3.27Å and 3.90Å, respectively), reminiscent of distances observed in **1ac**. This presumably is due to the steric requirements of two -OMe substituents on one of the rings as well as the twisted, non-planarity of the molecular backbone. Each molecule interacts with six neighboring molecules (Figure 6) *via* through-space interactions of the type (1) C-H$_{methoxy}$…O=C, (2) C-H$_{methoxy}$…O$_{nitro}$ and (3) the aromatic C-H of a nitrophenyl ring with a methoxy oxygen (Figure 6). These C-H…O interaction distances fall in a narrow 2.5-2.7Å range indicative of similarly weak electrostatic forces influencing the packing geometry of the molecules in the lattice.

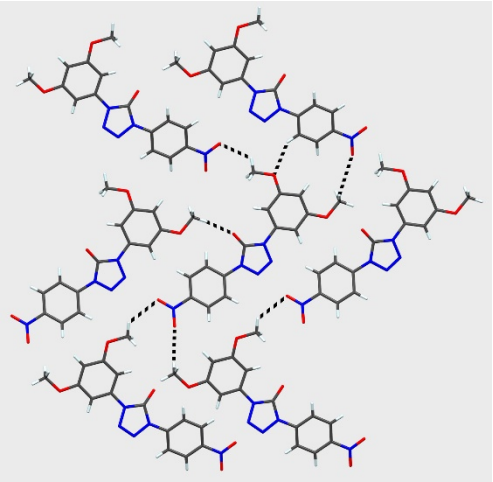

Figure 6. C-H…O interactions (distances in the 2.5 – 2.7Å range) present between molecules in the crystalline lattice of **1cl**.

Hirshfeld surface analysis. Hirshfeld surface analysis[47] of the structures of **1aa**, **1ac**, **1ad**, **1be$_{MeCN}$**, **1be$_{MeOH}$**, **1bk** and **1cl** revealed that predominantly surface contacts were typical van der Waals interactions. As might be expected, the majority are H…H contacts and will not be discussed further. Inspection of the surfaces of the molecules showed several regions on each molecule with significant, or slightly significant contacts (Figure 6). These contact regions, highlighted as "red" spots on the Hirshfeld surface map, are mainly between aromatic hydrogen atoms and either oxygen or nitrogen atoms (Table 3). Other significant contacts were between tetrazole nitrogen atoms and carbon atoms on neighboring molecules. For the six independent molecules in **1aa**, C…C intermolecular contacts also showed signs of close approach. This is not unexpected given the π-stacking present in the lattice. This is also true for **1ac** and **1be$_{MeCN}$**. However, **1be$_{MeOH}$** did not show any significant C…C interactions. Similarly, **1ad**, **1bk** and **1cl** had no dominant C…C contacts. Surprisingly, the surface map for **1cl** was relatively devoid of any significant interactions. For the fluorinated compounds **1be$_{MeCN}$** and **1be$_{MeOH}$**, fluorine impacts

the Hirshfeld surface and plays a role in many of the very close contacts observed in these two polymorphs. Figures depicting the molecules surrounding the core molecule or molecules that contribute to these interactions can be found in the supporting information Figures S6 – S12.

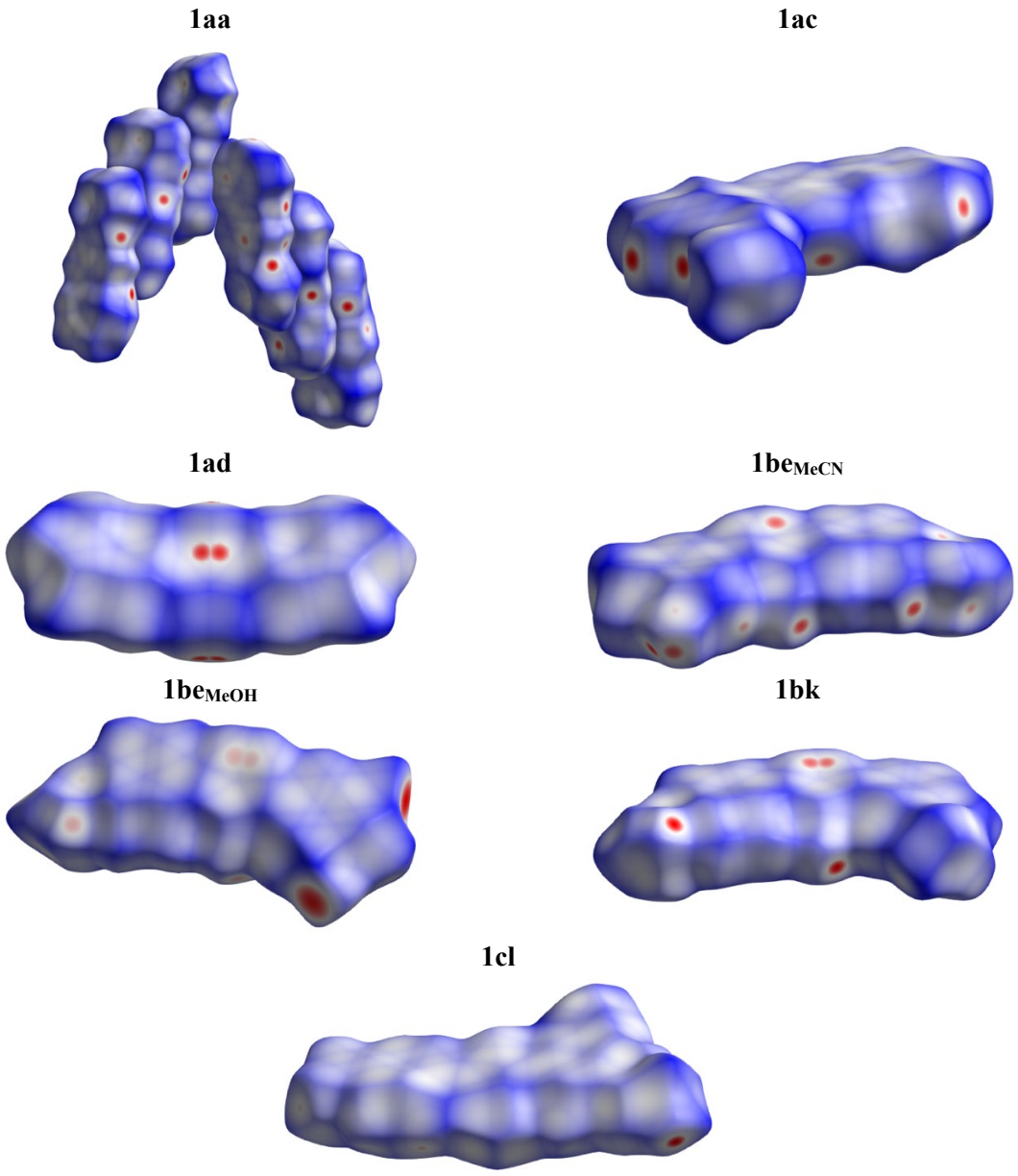

Figure 6. *Hirshfeld surface maps of* ***1aa****,* ***1ac****,* ***1ad, 1be****$_{MeCN}$,* ***1be****$_{MeOH}$,* ***1bk*** *and* ***1cl****. Close contacts are represented as red spots.*

Table 3. Hirshfeld surface analysis. Percent contribution to surface area contacts.[a]

Molecule	O···H	N···H	C···C	C···N	C···O	F···H	F···N
1aa 1	5.4	17.7	5.0	-	-	-	-
1aa 2	8.6	13.6	4.6	-	-	-	-
1aa 3	8.4	13.5	5.5	-	-	-	-
1aa 4	7.7	15.1	5.0	-	-	-	-
1aa 5	6.8	16.0	5.2	-	-	-	-
1aa 6	8.4	14.9	4.9	-	-	-	-
1ac	9.8	10.2	5.0	-	-	-	-
1ad	-	2.7	1.7	-	-	-	-
1be$_{MeCN}$	12.2	6.0	9.2	3.7	-	15.4	4.4
1be$_{MeOH}$	12.1	4.7	-	2.9	13.6	-	-
1bk	11.7	4.3	-	2.7	-	-	-
1cl	30.9	5.6	-	-	-	-	-

[a]*Contacts are given as inversion percentages. A dash indicates this is not a significant contribution to the strong interactions in a given molecule.*

Conclusions

We have reported an improved method for the synthesis of 1,4-diaryltetrazolones *via* C-N coupling of aryl tetrazolones and aryl boronic acids in the presence of Cu_2O nanoparticles under an oxygen atmosphere in DMSO as a solvent. This protocol provides substantial improvement over the previous method[22] as it uses relatively low catalyst loading, does not involve a base, requires short reaction times and produces higher yields. The reaction is generally insensitive to the nature and position of the substituents on the aryl tetrazolone or boronic acid, except in the case of *ortho* substituted aryl boronic acids where only a trace product was observed, possibly due to the steric hindrance encountered in coordination to the Cu during the catalytic cycle.[37] Due to

the relatively mild conditions, this method may be explored for its suitability in the formation of C-N bonds using other N-H containing motifs such as amines, amides, imidazoles, and indoles.

Furthermore, this is the first study that reports X-ray crystal structure analyses of 1,4-diaryltetrazolones. Our work revealed the presence of π..π stacking interactions between the adjacent layers in five of the seven structures. The assembly of molecules is further directed by weak electrostatic C-H…O interactions involving the neighboring pendant rings as well as the tetrazolone carbonyl and the pendant rings. Single crystals of **1bk** and **1be$_{MeOH}$**, differing only in the presence of a *p*-methyl or *p*-fluoro group, respectively, displayed an identical pattern of noncovalent interactions in the solid-state. In case of **1be$_{MeCN}$** and **1be$_{MeOH}$**, Hirshfeld surface analyses showed that fluorine plays a role in many of the very close contacts observed in these two polymorphs. We believe that the knowledge gained from this work, would stimulate further investigations on the crystal packing of this important class of compounds with potential to impact a variety of fields including medicinal, agricultural and materials chemistry.

Conflicts of interest

There are no conflicts to declare.

Acknowledgements

T.R. is grateful to the Ball State Honors College for the Undergraduate Honors Fellowship. Crystallographic data for **1aa**, **1ac**, **1bk**, and **1be$_{MeCN}$** and **1cl** were collected through the SCrALS (Service Crystallography at Advanced Light Source) program at Beamline 12.2.1 at the Advanced

Light Source, Lawrence Berkeley National Laboratory supported by the U.S. Department of Energy, Office of Energy Sciences Materials Sciences Division, under the contract DE-AC02-05CH11231. Crystal structure data for **1ad**, and **1be$_{MeOH}$** were collected at the University of Cincinnati on a D8 Venture diffractometer funded through NSF-MRI grant CHE-1625737. Mass spectrometric data were obtained on a Thermo Fisher LTQ XL supported by NSF-MRI grant under CHE-1531851. Acknowledgment is also made to the Donors of the American Chemical Society Petroleum Research Fund for the partial support of this research (ACS PRF # 61125-UR3). We acknowledge Dr. Allen G. Oliver, University of Notre Dame, for assistance with the Hirshfeld analyses.

Electronic Supplementary Information Available

Experimental procedures; TEM images of the nanoparticles; X-ray experimental description, overlayed single crystal structures as well as molecular and extended packing figures; molecular electrostatic potentials of remaining compounds; Hirshfeld surface analysis showing intermolecular interactions; ^{1}H and ^{13}C NMR spectra of all new compounds. CCDC 2052219-2052225 contain the supplementary crystallographic data for this paper. These data can be obtained free of charge via www.ccdc.cam.ac.uk/data_request/cif, or by emailing data_request@ccdc.cam.ac.uk, or by contacting The Cambridge Crystallographic Data Centre, 12 Union Road, Cambridge CB2 1EZ, UK; fax: +44 1223 336033

Notes and References

1. *WO Pat.,* 2017-US34613 2017205709, 2017.

2. *WO Pat.,* 2015-US18870 2015134699, 2015.
3. *WO Pat.,* 2011-US35141 2011140190, 2011.
4. *WO Pat.,* 2014-EP61527 2014198592, 2014.
5. *WO Pat.,* 2005-EP56951 2006067139, 2006.
6. T. L. Shih, M. R. Candelore, M. A. Cascieri, S.-H. L. Chiu, L. F. Colwell, Jr., L. Deng, W. P. Feeney, M. J. Forrest, G. J. Hom and D. E. MacIntyre, *Bioorg. Med. Chem. Lett.*, 1999, **9**, 1251-1254.
7. M. A. J. Duncton, R. B. Murray, G. Park and R. Singh, *Org. Biomol. Chem.*, 2016, **14**, 9343-9347.
8. Y. Matsuzaki, Y. Yoshimoto, S. Arimori, S. Kiguchi, T. Harada and F. Iwahashi, *Bioorg. Med. Chem.*, 2020, **28**, 115211.
9. G. Theodoridis, F. W. Hotzman, L. W. Scherer, B. A. Smith, J. M. Tymonko and M. J. Wyle, *Pestic. Sci.*, 1990, **30**, 259-274.
10. R. D. Clark, *ACS Symp. Ser.*, 1994, **559**, 34-47.
11. Y.-P. Luo, L. Lin and G.-F. Yang, *J. Heterocycl. Chem.*, 2007, **44**, 937-943.
12. Y.-P. Luo and G.-F. Yang, *Bioorg. Med. Chem.*, 2007, **15**, 1716-1724.
13. M.-Y. Jiang, L. Yu, Y.-C. Zhou, J. Jia, X.-J. Si, W.-W. Dong, Z.-F. Tian, J. Zhao and D.-S. Li, *Z. Anorg. Allg. Chem.*, 2020, **646**, 268-274.
14. X.-Y. Li, Z. Yin, W.-M. Ma, C. Wang, Y.-N. Yu and Y. Cheng, *Inorg. Chem. Commun.*, 2020, **116**, 107925.
15. R. Zhang, D.-X. Meng, F.-Y. Ge, J.-H. Huang, L.-F. Wang, Y.-K. Xv, X.-G. Liu, M.-M. Meng, H. Yan, Z.-Z. Lu, H.-G. Zheng and W. Huang, *Dalton Trans.*, 2020, **49**, 2145-2150.
16. P. He, J.-G. Zhang, K. Wang, X. Yin and T.-L. Zhang, *J. Phys. Org. Chem.*, 2016, **29**, 29-34.
17. P. He, L. Wu, J.-T. Wu, X. Yin, M. Gozin and J.-G. Zhang, *Dalton Trans.*, 2017, **46**, 8422-8430.
18. H. Noeth, K. Burger and W. Beck, *Z. Naturforsch., B J. Chem. Sci.*, 2011, **66**, 972-974.
19. F. Janssens, J. Torremans and P. A. J. Janssen, *J. Med. Chem.*, 1986, **29**, 2290-2297.
20. F. Janssens, J. Torremans, M. Janssen, R. A. Stokbroekx, M. Luyckx and P. A. J. Janssen, *J. Med. Chem*, 1985, **28**, 1934-1943.
21. A. Santhoshi, P. S. Sadhu, R. Sriram, C. N. S. S. P. Kumar, B. Mahendar, M. Sarangapani and V. J. Rao, *Med. Chem. Res.*, 2013, **22**, 3329-3340.
22. A. S. Gundugola, K. L. Chandra, E. M. Perchellet, A. M. Waters, J.-P. H. Perchellet and S. Rayat, *Bioorg. Med. Chem. Lett.*, 2010, **20**, 3920-3924.
23. *WO Pat.,* 2014-EP62521 2014202510, 2014.
24. H. Quast and U. Nahr, *Chem. Ber.*, 1985, **118**, 526-540.
25. H. Quast, A. Fuss and U. Nahr, *Chem. Ber.e*, 1985, **118**, 2164-2185.
26. R. Crockett, A. R. Forrester and R. A. Howie, *Acta Crystallogr., Sect. E Struct. Rep. Online*, 2003, **59**, o1347-o1348.
27. Y. Ohno, Y. Akutsu, M. Arai, M. Tamura, T. Matsunaga and M. Iida, *Acta Crystallogr., Sec. C: Cryst. Struct. Comm.*, 1998, **C54**, 1160-1162.
28. S. Rayat, O. Alawode and J. Desper, *CrystEngComm*, 2009, **11**, 1892-1898.

29. R. Y. Morjan, N. H. Al-Attar, O. S. Abu-Teim, M. Ulrich, A. M. Awadallah, A. M. Mkadmh, A. A. Elmanama, J. Raftery, F. M. Abu-Awwad, Z. J. Yaseen, A. F. Elqidrea and J. M. Gardiner, *Bioorg. Med. Chem. Lett.*, 2015, **25**, 4024-4028.
30. L. V. Kudzma, S. A. Severnak, M. J. Benvenga, E. F. Ezell, M. H. Ossipov, V. V. Knight, F. G. Rudo, H. K. Spencer and T. C. Spaulding, *J. Med. Chem.*, 1989, **32**, 2534-2542.
31. Y. V. Mel'nikova, L. V. Myznikov, A. V. Dogadina and N. I. Svintsitskaya, *Russ. J. Gen. Chem.*, 2014, **84**, 2160-2166.
32. G.-D. Zhang, Z. Wang, X. Yin and J.-G. Zhang, *Z. Anorg. Allg. Chem.*, 2018, **644**, 598-601.
33. O. Almarsson and M. J. Zaworotko, *Chem. Commun.*, 2004, 1889-1896.
34. N. Shan and M. J. Zaworotko, *Drug Discov. Today*, 2008, **13**, 440-446.
35. Y. Li, L.-X. Gao and F.-S. Han, *Chem. Commun.,* 2012, **48**, 2719-2721.
36. S. Rayat, R. Chhabra, O. Alawode and A. S. Gundugola, *J. Mol. Struct.*, 2009, **933**, 38-45.
37. C.-Y. Liu, Y. Li, J.-Y. Ding, D.-W. Dong and F.-S. Han, *Chem. - Eur. J.*, 2014, **20**, 2373-2381.
38. S. Monge, V. Darcos and D. M. Haddleton, *J. Polym. Sci., Part A Polym. Chem.*, 2004, **42**, 6299-6308.
39. S. Y. Moon, T. H. Noh and O.-S. Jung, *CrystEngComm*, 2013, **15**, 3854-3861.
40. B. Roldan Cuenya, *Acc. Chem. Res.*, 2013, **46**, 1682-1691.
41. L. Wu, Y. Zhang and Y.-G. Ji, *Curr. Org. Chem.*, 2013, **17**, 1288-1302.
42. Y. Li, E. Boone and M. A. El-Sayed, *Langmuir*, 2002, **18**, 4921-4925.
43. E. M. Zahran, N. M. Bedford, M. A. Nguyen, Y.-J. Chang, B. S. Guiton, R. R. Naik, L. G. Bachas and M. R. Knecht, *J. Am. Chem. Soc.*, 2014, **136**, 32-35.
44. Y.-H. Tsai, K. Chanda, Y.-T. Chu, C.-Y. Chiu and M. H. Huang, *Nanoscale*, 2014, **6**, 8704-8709.
45. M. J. Frisch, G. W. Trucks, H. B. Schlegel, G. E. Scuseria, M. A. Robb, J. R. Cheeseman, G. Scalmani, V. Barone, G. A. Petersson, H. Nakatsuji, X. Li, M. Caricato, A. Marenich, J. Bloino, B. G. Janesko, R. Gomperts, B. Mennucci, H. P. Hratchian, J. V. Ortiz, A. F. Izmaylov, J. L. Sonnenberg, D. Williams-Young, F. Ding, F. Lipparini, F. Egidi, J. Goings, B. Peng, A. Petrone, T. Henderson, D. Ranasinghe, V. G. Zakrzewski, J. Gao, N. Rega, G. Zheng, W. Liang, M. Hada, M. Ehara, K. Toyota, R. Fukuda, J. Hasegawa, M. Ishida, T. Nakajima, Y. Honda, O. Kitao, H. Nakai, T. Vreven, K. Throssell, J. Montgomery, J. A.; , J. E. Peralta, F. Ogliaro, M. Bearpark, J. J. Heyd, E. Brothers, K. N. Kudin, V. N. Staroverov, T. Keith, R. Kobayashi, J. Normand, K. Raghavachari, A. Rendell, J. C. Burant, S. S. Iyengar, J. Tomasi, M. Cossi, J. M. Millam, M. Klene, C. Adamo, R. Cammi, J. W. Ochterski, R. L. Martin, K. Morokuma, O. Farkas, J. B. Foresman and D. J. Fox, *Gaussian 09*, Gaussian Inc., Pittsburg, PA, 2009.
46. R. Dennington, T. Keith and J. Millam, *GaussView, Version 5*, Semichem Inc., Shawnee Mission, KS, 2009.
47. M. A. Spackman and D. Jayatilaka, *CrystEngComm*, 2009, **11**, 19-32.